

Decisive role of electron-phonon coupling for phonon and electron instabilities in transition metal dichalcogenides

Zishen Wang,^{1,2,*} Chuan Chen,^{3,4,*} Jinchao Mo,¹ Jun Zhou,^{5,†} Kian Ping Loh,^{2,6,‡} and Yuan Ping Feng^{1,2,§}

¹*Department of Physics, National University of Singapore, 117542 Singapore, Singapore*

²*Centre for Advanced 2D Materials, National University of Singapore, 117546 Singapore, Singapore*

³*Institute for Advanced Study, Tsinghua University, 100084 Beijing, China*

⁴*Max-Planck Institute for the Physics of Complex Systems, 01187 Dresden, Germany*

⁵*Institute of Materials Research & Engineering, A*STAR (Agency for Science, Technology and Research), 138634 Singapore, Singapore.*

⁶*Department of Chemistry, National University of Singapore, 117543 Singapore, Singapore*

The origin of the charge density wave (CDW) in transition metal dichalcogenides has been in hot debate and no conclusive agreement has been reached. Here, we propose an *ab-initio* framework for an accurate description of both Fermi surface nesting and electron-phonon coupling (EPC) and systematically investigate their roles in the formation of CDW. Using monolayer 1H-NbSe₂ and 1T-VTe₂ as representative examples, we show that it is the momentum-dependent EPC softens the phonon frequencies, which become imaginary (phonon instabilities) at CDW vectors (indicating CDW formation). Besides, the distribution of the CDW gap opening (electron instabilities) can be correctly predicted only if EPC is included in the mean-field model. These results emphasize the decisive role of EPC in the CDW formation. Our analytical process is general and can be applied to other CDW systems.

The formation of charge density wave (CDW) is a spontaneous symmetry breaking process with periodic charge density modulations and lattice distortions below a critical temperature (T_{CDW}) [1, 2]. However, the origin of CDW is a long-standing problem, which attracts broad research interest in condensed matter physics [3–6]. The first mechanism, Fermi surface nesting (FSN), was originated from Peierls’ model of an ideal one-dimensional (1D) metal atomic chain. FSN relates to an elastic electronic scattering at the Fermi surface [7]. The zero-energy electronic excitations screen the phonon vibration at the CDW vector \mathbf{Q} , inducing an abrupt phonon softening (known as Kohn anomaly) [8]. However, the extension of FSN to real materials is not ideal. With a few exceptions, FSN is argued to have limited power in inducing CDW distortions in higher-dimensional systems [4–6, 9].

Instead, momentum-dependent electron-phonon coupling (\mathbf{q} -EPC), which involves an inelastic electronic scattering mediated by a phonon, is argued to be more prevailing in higher-dimensional systems [4–6, 9]. In an electron-phonon interaction dominant system, the electron field can be integrated out as a perturbation to the free phonon field, softening phonon frequencies from their bare values [see SI-III for details]. Thus, both FSN and \mathbf{q} -EPC may soften phonons to imaginary values (phonon instabilities) and induce CDW distortions. However, quantitative studies of \mathbf{q} -EPC are rare, and the reported method to directly obtain \mathbf{q} -EPC is a tight-binding model by merely using the electronic band structure [10–12]. Besides, such a semi-empirical method is hard to give rigorous results compared to the first-principles calculations. Therefore, it is imperative to explore a general method to accurately describe \mathbf{q} -EPC in the CDW ma-

terials.

Another important feature of a CDW is the band gap opening (electron instabilities) accompanied by the CDW distortions, which lowers the energy of the system [2, 4, 13]. The location of the CDW gap in the Brillouin zone (BZ) can be identified accurately by a band unfolding scheme [14–16], which however requires the prior knowledge of the corresponding CDW structure and cannot provide insight into the underlying mechanism. Thus, the driving force of the CDW gap is still elusive. A convenient method that can give physical insight into the gap opening is needed.

In this letter, we use monolayer 1H-NbSe₂ and 1T-VTe₂ (in short NbSe₂ and VTe₂) as representative examples for the most common high-symmetry phases of the transition metal dichalcogenides (TMDs). Another reason for such a choice is the mechanisms of their CDWs are considered to be different. The electron-phonon coupling (EPC) has been shown to be dominant in NbSe₂ [15, 17, 18], while FSN in VTe₂ seems to be substantial, which leads to a peak in the static Lindhard susceptibility [19, 20]. Thus, we conduct a comprehensive study of their CDW properties from both phononic and electronic perspectives. In the phononic part, we obtain the accurate \mathbf{q} -EPC from the fully first-principles calculations, which allows us to make a straightforward comparison between the contributions from FSN and \mathbf{q} -EPC in the CDW formation. Interestingly, the \mathbf{q} -EPC is shown to play the dominant role in designating the CDW vectors for both NbSe₂ and VTe₂. While in the electronic part, we find the rigorous EPC matrix elements are the key to predict the distribution of the CDW gaps by our mean-field model. In addition, we argue that our analysis process, besides its conciseness and accurateness, should be

a general framework, which can be easily exploited in other CDW systems.

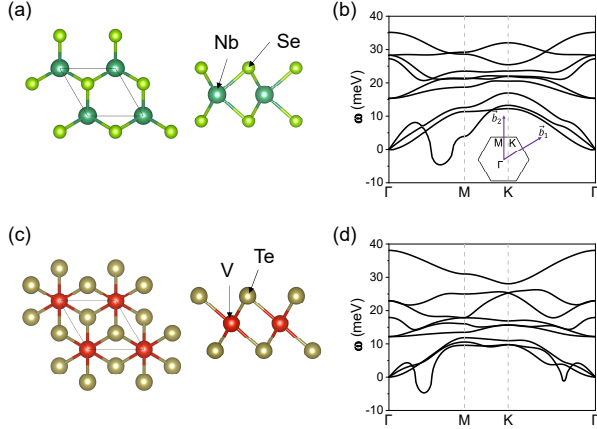


FIG. 1. (a) Top and side views of the crystal structure, (b) phonon dispersion of monolayer 1H-NbSe₂. (c, d) Same as panel (a, b) but for monolayer 1T-VTe₂. The insert figure in (b) displays the first BZ with reciprocal lattice vectors.

Phonon instabilities and CDW mechanism.—TMDs have layered structures, in which transition metal atoms are sandwiched by chalcogen atoms, forming trigonal prisms (a 1H phase) or octahedrons (a 1T phase). The structures of 1H-NbSe₂ and 1T-VTe₂ are shown in Figs. 1(a) and 1(c), respectively. As the phonon spectra for NbSe₂ and VTe₂ shown in Figs. 1(b) and 1(d), their longitudinal acoustic (LA) phonon modes collapse at the CDW vectors, which triple the unit cell for NbSe₂ with $\mathbf{Q}^H = 2/3\Gamma M$, and quadruple the unit cell for VTe₂ with $\mathbf{Q}^T = 1/2\Gamma M$, in line with the CDW supercells obtained from experiments [19, 21–23].

To account for the driving force of the phonon softening, the relationship between the softened phonon frequency $\omega_{\mathbf{q}}$ and its bare phonon frequency $\Omega_{\mathbf{q}}$ is described under the random phase approximation (RPA) [See more details in SI-III]:

$$\omega_{\mathbf{q}}^2 = \Omega_{\mathbf{q}}^2 - 2\Omega_{\mathbf{q}}\chi_{\mathbf{q}} \quad (1)$$

where $\chi_{\mathbf{q}}$ is the generalized static electronic susceptibility, including both contributions from FSN and EPC, which is given by:

$$\chi_{\mathbf{q}} = \sum_{\mathbf{k}} |g_{\mathbf{k},\mathbf{k}+\mathbf{q}}|^2 \frac{f(\varepsilon_{\mathbf{k}}) - f(\varepsilon_{\mathbf{k}+\mathbf{q}})}{\varepsilon_{\mathbf{k}+\mathbf{q}} - \varepsilon_{\mathbf{k}}} \quad (2)$$

where $f(\varepsilon)$ is the Fermi-Dirac function of the eigenvalue ε , $g_{\mathbf{k},\mathbf{k}+\mathbf{q}}$ is the electron-phonon coupling matrix element that couples electronic states \mathbf{k} and $\mathbf{k}+\mathbf{q}$ with a phonon of momentum \mathbf{q} . According to eq. (1), the ordering vector is estimated from the maximum of $\chi_{\mathbf{q}}$ [11, 12]. The $\chi_{\mathbf{q}}$ often reduces to the static Lindhard susceptibility $\chi'_{\mathbf{q}}$ under the constant matrix element approximation ($|g_{\mathbf{k},\mathbf{k}+\mathbf{q}}| = 1$):

$$\chi'_{\mathbf{q}} = \sum_{\mathbf{k}} \frac{f(\varepsilon_{\mathbf{k}}) - f(\varepsilon_{\mathbf{k}+\mathbf{q}})}{\varepsilon_{\mathbf{k}+\mathbf{q}} - \varepsilon_{\mathbf{k}}} \quad (3)$$

which is a pure electron effect, and its peak reflects the electronic instability by FSN [4]. Similarly, $\chi_{\mathbf{q}}$ can reduce to the \mathbf{q} -EPC $\bar{g}_{\mathbf{q}}$ under the “constant fraction” approximation ($\frac{f(\varepsilon_{\mathbf{k}}) - f(\varepsilon_{\mathbf{k}+\mathbf{q}})}{\varepsilon_{\mathbf{k}+\mathbf{q}} - \varepsilon_{\mathbf{k}}} = 1$):

$$\bar{g}_{\mathbf{q}} = \sum_{\mathbf{k}} |g_{\mathbf{k},\mathbf{k}+\mathbf{q}}|^2 \quad (4)$$

which reflects a pure EPC effect. Focusing on the low energy interaction around the Fermi level, we only consider the coupling between the lowest phonon branch and the single electronic band which crosses the Fermi level [see the pink bands in Figs. S1(b) and S1(e)]. Due to the complexity in describing the EPC matrix elements, only static Lindhard susceptibility has been widely used to understand the CDW formation, while the \mathbf{q} -EPC which however may play a more important role is ignored [4, 6].

Here, to remedy this blemish, we applied density functional perturbation theory (DFPT) to obtain the accurate element g , which is given by [24]:

$$g_{\mathbf{k},\mathbf{k}+\mathbf{q}} = \left(\frac{\hbar}{2M\omega_{\mathbf{q}}}\right)^{1/2} \langle \varphi_{\mathbf{k}+\mathbf{q}} | \partial_{\mathbf{q}} V | \varphi_{\mathbf{k}} \rangle \quad (5)$$

where $\partial_{\mathbf{q}} V$ is the derivative of the electron-ion potential with phonon frequency $\omega_{\mathbf{q}}$, $\varphi_{\mathbf{k}}$ is the electronic wavefunction with wavevector \mathbf{k} . For a direct comparison, we also calculated the matrix element g between electronic states \mathbf{k} and $\mathbf{k}+\mathbf{q}$ by the tight-binding (TB) model [10–12], which is:

$$g_{\mathbf{k},\mathbf{k}+\mathbf{q}} \propto (\nu_{\mathbf{k}} - \nu_{\mathbf{k}+\mathbf{q}}) \cdot \frac{\mathbf{q}}{|\mathbf{q}|} \quad (6)$$

where $\nu_{\mathbf{k}}$ is the electron velocity at \mathbf{k} point in the coupled band, $\frac{\mathbf{q}}{|\mathbf{q}|}$ is the longitudinal projection as only LA phonons soften to zero. And this method succeeded in describing EPC properties in bulk 2H-NbSe₂ [11, 12] and monolayer 1T-VSe₂ [25]. To distinguish the two different sources of EPC matrix elements in the following discussions, the related quantities obtained by the TB method are denoted as $\bar{g}_{\mathbf{q}}^{TB}$ and $\chi_{\mathbf{q}}^{TB}$, while the quantities obtained by DFPT are used bare notation $\bar{g}_{\mathbf{q}}$ and $\chi_{\mathbf{q}}$.

The calculated $\chi'_{\mathbf{q}}$, $\bar{g}_{\mathbf{q}}$, $\chi_{\mathbf{q}}$, and $\omega_{\mathbf{q}}$ for NbSe₂ (upper panels) and VTe₂ (lower panels) are shown in Fig. 2. For NbSe₂, the static Lindhard susceptibility $\chi'_{\mathbf{q}}$ has a broad plateau from $2/5\Gamma M$ to $4/5\Gamma M$ [see Fig. 2(a) and the blue line in Fig. 3(a)], which indicates the weakness of FSN [18]. Nonetheless, $\bar{g}_{\mathbf{q}}$ shows a strong electron-phonon interaction near $2/3\Gamma M$ for NbSe₂ [see Fig. 2(b)

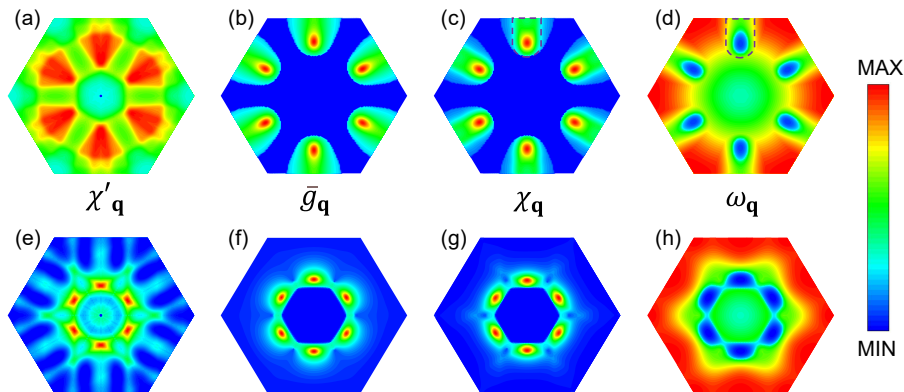


FIG. 2. (a) Static Lindhard susceptibility $\chi'_{\mathbf{q}}$, (b) \mathbf{q} -EPC $\bar{g}_{\mathbf{q}}$, (c) generalized static electronic susceptibility $\chi_{\mathbf{q}}$ and (d) the lowest phonon frequency $\omega_{\mathbf{q}}$ in the first BZ of NbSe₂. (e-h) Same as panel (a-d) but for VTe₂.

and the red line in Fig. 3(a)]. In addition, the topology of $\chi_{\mathbf{q}}$ is very similar to $\bar{g}_{\mathbf{q}}$ [Figs. 2(b) and 2(c)] in the NbSe₂ first BZ, indicating the dominated role played by the \mathbf{q} -EPC in $\chi_{\mathbf{q}}$. Fig. 2(d) displays the softened phonon modes of NbSe₂, which are concentrated in the arch-like area [see the purple dashed line in Fig. 2(d)], in agreement with the highland in $\chi_{\mathbf{q}}$ [see the purple dashed line in Fig. 2(c)]. More importantly, the peaks in $\bar{g}_{\mathbf{q}}$ and $\chi_{\mathbf{q}}$ [see the red areas in Figs. 2(b) and 2(c)] are at $2/3\Gamma M$, which is consistent with the dip in $\omega_{\mathbf{q}}$ [see the blue areas in Fig. 2(d)].

The EPC properties of bulk 2H-NbSe₂ have been well-described by using the TB method [11, 12], however, we find this method fails in addressing monolayer 1H-NbSe₂. As for the generalized static electronic susceptibility $\chi_{\mathbf{q}}^{TB}$, the overall topology in the first BZ [Fig. S3(c)] cannot fit the phonon softening [Fig. 2(d)], which is in stark contrast to the good match achieved by DFPT [Fig. 2(c)]. Besides, the peaks of $\bar{g}_{\mathbf{q}}^{TB}$ and $\chi_{\mathbf{q}}^{TB}$ at the ΓM path [see the green line in Fig. 3(a) and the orange line in Fig. 3(b)] are near $1/2\Gamma M$, which predict the formation of 4×4 CDW instead of 3×3 CDW. By comparing to the prominent peaks of $\bar{g}_{\mathbf{q}}$ and $\chi_{\mathbf{q}}$ at $2/3\Gamma M$ obtained by the DFPT [see the red line in Fig. 3(a) and the black line in Fig. 3(b)], we conclude that the *ab-initio* based DFPT method is superior to the TB method in obtaining the \mathbf{q} -EPC and predicting the CDW vector in monolayer NbSe₂.

For monolayer VTe₂, $\chi'_{\mathbf{q}}$ has a peak near $2/5\Gamma M$ [see Fig. 2(e) and the blue line in Fig. 3(c)], in line with previous works [19, 20]. However, this peak does not correspond to the 4×4 CDW structure observed from the experiments [19, 23]. Besides, the profile of $\chi_{\mathbf{q}}$ in the first BZ is again very close to $\bar{g}_{\mathbf{q}}$ [Figs. 2(f) and 2(g)], which both show maxima close to $1/2\Gamma M$, providing a powerful clue of phonon softening at \mathbf{Q}^T . As shown in Fig. 2(h), the distribution of the softened phonon frequency $\omega_{\mathbf{q}}$ of VTe₂ shows hexapetalous flower-like pattern [see the blue area in Fig. 2(h)], which match well with the

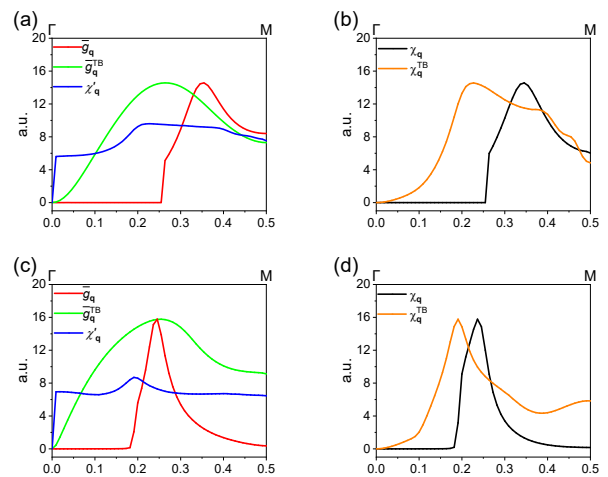


FIG. 3. Direct comparison of the role of EPC and FSN along ΓM path in NbSe₂ (up panel) and VTe₂ (down panel). (a) Comparing the difference among $\bar{g}_{\mathbf{q}}$ (red), $\bar{g}_{\mathbf{q}}^{TB}$ (green) and $\chi'_{\mathbf{q}}$ (blue) in NbSe₂, (b) Comparing the difference between $\chi_{\mathbf{q}}$ (black) and $\chi_{\mathbf{q}}^{TB}$ (orange) in NbSe₂. (c, d) Same as panels (a, b), but for VTe₂. Note that the unit of the y-coordinate is arbitrary units (a.u.) for straightforward comparison.

“hot” area in $\chi_{\mathbf{q}}$ [Fig. 2(g)]. One should note that the peak of $\bar{g}_{\mathbf{q}}$ is very sharp, which overwhelms the fluctuation of $\chi'_{\mathbf{q}}$ in VTe₂ [see the red line and the blue line in Fig. 3(c)], leading to the correct $1/2\Gamma M$ peak position of $\chi_{\mathbf{q}}$ [see the black line in Fig. 3(d)]. However, the TB method still cannot explain the phonon softening in VTe₂. Although $\bar{g}_{\mathbf{q}}^{TB}$ shows a peak at $1/2\Gamma M$, such peak is even broader than the nesting peak at $2/5\Gamma M$, leading to the incorrect peak position of $\chi_{\mathbf{q}}^{TB}$ at $2/5\Gamma M$ [see the green line in Fig. 3(c) and the orange line in Fig. 3(d)]. Compared the distribution of $\bar{g}_{\mathbf{q}}^{TB}$ [Fig. S3(e)], the “sharpness” of $\chi'_{\mathbf{q}}$ make the topology of $\chi_{\mathbf{q}}^{TB}$ closer to that of the $\chi'_{\mathbf{q}}$ in the first BZ of VTe₂ [Figs. 2(e) and S3(f)], which cannot explain the phonon softening

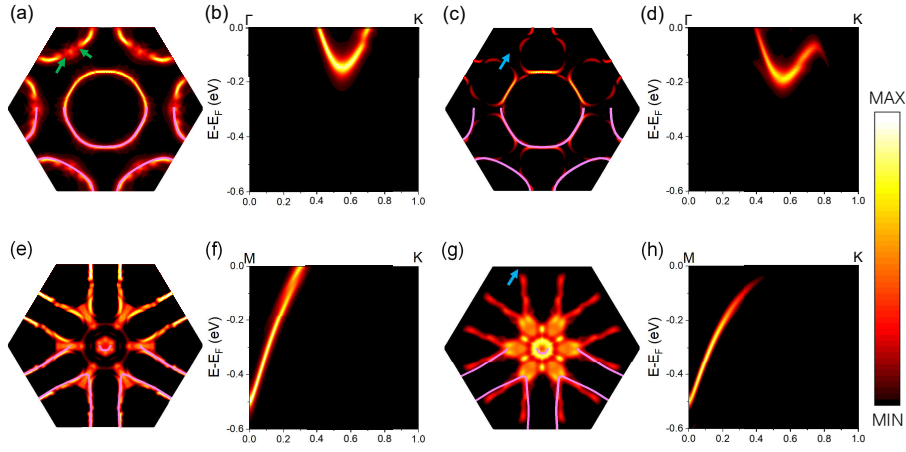


FIG. 4. Simulation of the (a) Fermi surface and (b) the spectral function along ΓK direction with constant $|g|$ of the NbSe₂ CDW system. (c, d) Same as (a, b), but with anisotropic g in the simulation. Simulation of the (e) Fermi surface and (f) the spectral function along MK direction with constant $|g|$ of the VTe₂ CDW system. (g, h) Same as (e, f), but with anisotropic g in the simulation. The brightness of the dots denotes the spectral weights. The pink solid lines in (a, c, e, g) in the lower half of the BZ are the corresponding non-CDW Fermi surfaces for comparison. The green arrows in (a) indicate the partial CDW gaps opened by FSN, the blue arrows in (c, g) indicate the full CDW gaps opened by FSN + EPC. The paths of the spectral functions are chosen to better show the full CDW gaps.

shown in Fig. 2(h). Therefore, with the help of the accurate EPC matrix element g obtained by DFPT, our study clearly demonstrates that it is \mathbf{q} -EPC rather than FSN determines the phonon softening at correct positions and accounts for the CDW formation in both NbSe₂ and VTe₂.

Electron instabilities and CDW gaps.—Having identified the domination of EPC in phonon softening, we now study the momentum-dependent CDW gap (electron instabilities) based on mean-field theory. The Hamiltonian of the CDW phase is minimally described by including one band crossing the Fermi level and electron-phonon interaction with phonon momentum \mathbf{Q} .

$$H_{mf} = \sum_{\mathbf{k}} \varepsilon_{\mathbf{k}} c_{\mathbf{k}}^{\dagger} c_{\mathbf{k}} + \sum_{\mathbf{k}, \mathbf{Q}} 2g_{\mathbf{k}, \mathbf{k}+\mathbf{Q}} \Delta_{\mathbf{Q}} c_{\mathbf{k}}^{\dagger} c_{\mathbf{k}+\mathbf{Q}} + h.c. \quad (7)$$

Here, $c_{\mathbf{k}}^{\dagger}$ ($c_{\mathbf{k}}$) and $\varepsilon_{\mathbf{k}}$ are creation (annihilation) operator and energy for an electron with momentum \mathbf{k} . $\Delta_{\mathbf{Q}}$ is the order parameter which was approximated to a constant because of symmetry and small pocket size. This Hamiltonian can then be used to calculate the spectral function of the CDW phases [see SI-IV for more details about the theoretical background].

As shown in Fig. 4(a), the simulated Fermi surface of the NbSe₂ CDW structure with constant EPC matrix elements $|g|$ (i.e., $|g| = \sum_{\mathbf{k}, \mathbf{k}+\mathbf{Q}} |g_{\mathbf{k}, \mathbf{k}+\mathbf{Q}}| / N_{\mathbf{k}, \mathbf{k}+\mathbf{Q}}$, where $N_{\mathbf{k}, \mathbf{k}+\mathbf{Q}}$ is the number of g in the calculation.) reflects the FSN effect under the mean-field picture. The norm of g is used to avoid the arbitrary phase factor problem in the band basis of EPC matrix element. It is clearly shown that each K pocket has 3 couples of partial gaps [see the

green arrows in Fig. 4(a)], where the spectral intensity becomes blurred as only partial electronic states are left at the Fermi surface. The partial gaps are at both sides of the ΓK path, corresponding to the most heavily nested points of NbSe₂ [see the red points in white circle in Fig. S6(c)]. The incorporation of anisotropic matrix elements g develop a more extensive gap opening on the Fermi surface [Fig. 4(c)], which considers the synergistic effects of FSN and EPC. Remarkably, the full band-gapped sectors can be found on the K pockets, where the electronic states on the Fermi surface are completely obliterated [see the blue arrow in Fig. 4(c)]. Furthermore, the spectral function was plotted along the ΓK path, and we find the pure nesting effect cannot open a band gap along this path [Fig. 4(b)], in contrast with the spectral function derived with the anisotropic g , which obviously displays a full band gap close to the K point [Fig. 4(d)]. Considering there is no experimental report on the Fermi surface of the monolayer NbSe₂ CDW state, the predicted CDW gap distribution is compared with the unfolded Fermi surface of the simulated NbSe₂ CDW ground state, which displays a remarkable agreement with each other [14, 17].

It is known that VTe₂ has triangular hole pockets, which has parallel sides to provide good nesting condition [19, 20]. Such nesting will induce a peak in the static Lindhard susceptibility and possibly open a gap at the heavily nested point [19]. In the phononic part discussion, FSN as the mechanism of the phonon softening in VTe₂ has been excluded, we now turn to discuss its relation to the CDW gap. Fig. 4(e) suggests that there is no obvious spectral weight depletion on the Fermi surface, and no CDW gap can be opened at the MK path [Figs. 4(e) and 4(f)]. However, after considering the effect of

the anisotropic EPC matrix elements g , there is a strong suppression of the spectral intensity near the M point [see the blue arrow in Fig. 4(g)]. No electronic state can be found on the Fermi surface at the MK path, which indicates a full gap opening [Fig. 4(h)], consistent with the recent experimental results [19]. Moving toward the Γ point, the decreasing of the gap size is accompanied by the full to partial gap transition, and finally the gap is closed at the triangular K pocket apex [see Fig. 4(g)]. Such an anisotropic gap distribution on the Fermi surface agrees well with the angle-resolved photoemission spectroscopy (ARPES) measurements [19].

Discussion.—Although the CDW formation has been widely studied for decades, the underlying mechanism is still under debate. Using NbSe₂ and VTe₂ as examples, we explore the origin of their CDW orders by providing a comprehensive *ab-initio* theoretical study. This study is vital because it is difficult to reconcile FSN and EPC so far. The main features of this work include an accurate description of the \mathbf{q} -EPC in the whole BZ for the first time, correctly calculating the generalized static electronic susceptibility, the understanding of the CDW formation mechanism, and comparing the CDW gap distribution by the mean-field model with or without incorporating the EPC effects. All these results are self-consistent and emphasize the importance of EPC.

We also address some puzzles surrounding the CDW properties of monolayer NbSe₂ and VTe₂. For monolayer NbSe₂, a small CDW gap of 4 meV is obtained by the molecular-beam epitaxy (MBE) grown samples with low $T_{CDW} \sim 25\text{K}$ [21]. While the mechanically exfoliated samples show higher $T_{CDW} \sim 145\text{K}$ without a gap measurement [26, 27], and it is believed that a large T_{CDW} corresponds to a large gap size [1, 2, 11, 16]. Previous experimental and theoretical studies indicate that the suppression of the 3×3 CDW order in the MBE-grown NbSe₂ samples is due to the charge transfer from the graphene substrate [26, 28, 29]. Therefore, the intrinsic NbSe₂ is expected to have a larger gap size than 4meV, as revealed by the previous unfolded band structure [14, 15] and our mean-field simulation. For monolayer VTe₂, previous work reported that there is no observable charge transfer between VTe₂ samples and the graphene substrate [20], hence, the graphene based VTe₂ samples may be close to the freestanding one, which should have similar properties including the CDW gap opening. Our mean-field calculations successfully reproduce the experimental ARPES results as expected [19]. Besides, the long parallel sides of the triangular hole pockets provide a good condition for FSN, which was thought to be the origin of the anisotropic CDW gap [19]. However, our work excludes this hypothesis and emphasizes the significance of EPC in the CDW gap opening by providing a convincing description.

In conclusion, using first-principles calculations and the mean-field theory, we report a quantitative study of

CDW properties in monolayer 1H-NbSe₂ and 1T-VTe₂. Our results confirm the validity of the EPC mechanism in a non-1D CDW system, which supplies previous experimental and theoretical works. The combined analysis of FSN and EPC in both phononic and electronic pictures constructs a profound understanding of the CDW formation mechanism. We argue that the same physics, in principle, should be applied to other higher-dimensional CDW systems. Besides, the proposed analytical method can be decorated by more accurate calculations (i.e., GGA+U, GW, hybrid function, etc.) [24, 30–32], which allows further CDW studies in more complex systems. Our work paves a general way to unravel the physical insights of the CDW formation mechanism with phonon and electron instabilities, which can be extended for the understanding of charge ordering in other transition metal compounds [33], kagome metals [34] and high-temperature superconductors [35].

Acknowledgement.— Z.W. thanks Dr. Felix Flicker for fruitful discussions. Z.W. also thanks Dr. Miguel Dias Costa and Yi-Ming Zhao for IT support. C.C. acknowledges the support from Shuimu Tsinghua Scholar Program. This research project is partially supported by the Ministry of Education, Singapore, under its MOE AcRF Tier 3 Award MOE2018-T3-1-002, and MOE AcRF Tier 2 Award MOE2019-T2-2-030. Numerical computations were supported by the National Supercomputing Center (NSCC) Singapore and Center of Advanced 2D Materials (CA2DM) HPC infrastructure.

* These authors contributed equally.

† zhou.jun@imre.a-star.edu.sg

‡ chmlhkp@nus.edu.sg

§ phyfyp@nus.edu.sg

- [1] G. Grüner, The dynamics of charge-density waves, *Reviews of modern physics* **60**, 1129 (1988).
- [2] K. Rossnagel, On the origin of charge-density waves in select layered transition-metal dichalcogenides, *Journal of Physics: Condensed Matter* **23**, 213001 (2011).
- [3] X. Zhu, J. Guo, J. Zhang, and E. Plummer, Misconceptions associated with the origin of charge density waves, *Advances in Physics: X* **2**, 622 (2017).
- [4] M. D. Johannes and I. I. Mazin, Fermi surface nesting and the origin of charge density waves in metals, *Physical Review B* **77**, 165135 (2008).
- [5] F. Weber, S. Rosenkranz, J.-P. Castellan, R. Osborn, R. Hott, R. Heid, K.-P. Bohnen, T. Egami, A. H. Said, and D. Reznik, Extended phonon collapse and the origin of the charge-density wave in 2 h- nbse 2, *Physical review letters* **107**, 107403 (2011).
- [6] X. Zhu, Y. Cao, J. Zhang, E. Plummer, and J. Guo, Classification of charge density waves based on their nature, *Proceedings of the National Academy of Sciences* **112**, 2367 (2015).
- [7] R. E. Peierls, *Quantum theory of solids* (Oxford Univer-

- sity Press, 1955).
- [8] W. Kohn, Image of the fermi surface in the vibration spectrum of a metal, *Physical Review Letters* **2**, 393 (1959).
- [9] J. Diego, A. Said, S. Mahatha, R. Bianco, L. Monacelli, M. Calandra, F. Mauri, K. Rossnagel, I. Errea, and S. Blanco-Canosa, van der waals driven anharmonic melting of the 3d charge density wave in vse 2, *Nature communications* **12**, 598 (2021).
- [10] C. M. Varma, E. I. Blount, P. Vashishta, and W. Weber, Electron-phonon interactions in transition metals, *Physical Review B* **19**, 6130 (1979).
- [11] F. Flicker and J. Van Wezel, Charge order from orbital-dependent coupling evidenced by nbse 2, *Nature communications* **6**, 1 (2015).
- [12] F. Flicker and J. van Wezel, Charge order in nbse 2, *Physical Review B* **94**, 235135 (2016).
- [13] Z. Wang, J. Zhou, K. P. Loh, and Y. P. Feng, Controllable phase transitions between multiple charge density waves in monolayer 1t-vse2 via charge doping, *Applied Physics Letters* **119**, 163101 (2021).
- [14] F. Zheng, Z. Zhou, X. Liu, and J. Feng, First-principles study of charge and magnetic ordering in monolayer nbse 2, *Physical Review B* **97**, 081101(R) (2018).
- [15] C.-S. Lian, C. Si, and W. Duan, Unveiling charge-density wave, superconductivity, and their competitive nature in two-dimensional nbse2, *Nano letters* **18**, 2924 (2018).
- [16] P. Chen, W. W. Pai, Y.-H. Chan, V. Madhavan, M.-Y. Chou, S.-K. Mo, A.-V. Fedorov, and T.-C. Chiang, Unique gap structure and symmetry of the charge density wave in single-layer vse 2, *Physical review letters* **121**, 196402 (2018).
- [17] F. Zheng and J. Feng, Electron-phonon coupling and the coexistence of superconductivity and charge-density wave in monolayer nbse 2, *Physical Review B* **99**, 161119(R) (2019).
- [18] M. Calandra, I. I. Mazin, and F. Mauri, Effect of dimensionality on the charge-density wave in few-layer 2h-nbse2, *Physical Review B* **80**, 241108(R) (2009).
- [19] Y. Wang, J. Ren, J. Li, Y. Wang, H. Peng, P. Yu, W. Duan, and S. Zhou, Evidence of charge density wave with anisotropic gap in a monolayer vte 2 film, *Physical Review B* **100**, 241404(R) (2019).
- [20] K. Sugawara, Y. Nakata, K. Fujii, K. Nakayama, S. Souma, T. Takahashi, and T. Sato, Monolayer vte 2: Incommensurate fermi surface nesting and suppression of charge density waves, *Physical Review B* **99**, 241404(R) (2019).
- [21] M. M. Ugeda, A. J. Bradley, Y. Zhang, S. Onishi, Y. Chen, W. Ruan, C. Ojeda-Aristizabal, H. Ryu, M. T. Edmonds, H.-Z. Tsai, *et al.*, Characterization of collective ground states in single-layer nbse 2, *Nature Physics* **12**, 92 (2016).
- [22] Y. Nakata, K. Sugawara, S. Ichinokura, Y. Okada, T. Hitosugi, T. Koretsune, K. Ueno, S. Hasegawa, T. Takahashi, and T. Sato, Anisotropic band splitting in monolayer nbse 2: Implications for superconductivity and charge density wave, *npj 2D Materials and Applications* **2**, 12 (2018).
- [23] P. M. Coelho, K. Lasek, K. Nguyen Cong, J. Li, W. Niu, W. Liu, I. I. Oleynik, and M. Batzill, Monolayer modification of vte2 and its charge density wave, *The journal of physical chemistry letters* **10**, 4987 (2019).
- [24] F. Giustino, Electron-phonon interactions from first principles, *Reviews of Modern Physics* **89**, 015003 (2017).
- [25] R. Chua, J. Henke, S. Saha, Y. Huang, J. Gou, X. He, T. Das, J. van Wezel, A. Soumyanarayanan, and A. T. Wee, Coexisting charge-ordered states with distinct driving mechanisms in monolayer vse2, *ACS nano* **16**, 783 (2021).
- [26] D. Lin, S. Li, J. Wen, H. Berger, L. Forró, H. Zhou, S. Jia, T. Taniguchi, K. Watanabe, X. Xi, *et al.*, Patterns and driving forces of dimensionality-dependent charge density waves in 2 h-type transition metal dichalcogenides, *Nature communications* **11**, 2406 (2020).
- [27] X. Xi, L. Zhao, Z. Wang, H. Berger, L. Forró, J. Shan, and K. F. Mak, Strongly enhanced charge-density-wave order in monolayer nbse 2, *Nature nanotechnology* **10**, 765 (2015).
- [28] J. Á. Silva-Guillén, P. Ordejón, F. Guinea, and E. Canadell, Electronic structure of 2h-nbse2 single-layers in the cdw state, *2D Materials* **3**, 035028 (2016).
- [29] Y. Chen, L. Wu, H. Xu, C. Cong, S. Li, S. Feng, H. Zhang, C. Zou, J. Shang, S. A. Yang, *et al.*, Visualizing the anomalous charge density wave states in graphene/nbse2 heterostructures, *Advanced Materials* **32**, 2003746 (2020).
- [30] J.-J. Zhou, J. Park, I. Timrov, A. Floris, M. Cococcioni, N. Marzari, and M. Bernardi, Ab initio electron-phonon interactions in correlated electron systems, *Physical review letters* **127**, 126404 (2021).
- [31] Z. Li, G. Antonius, M. Wu, F. H. daJornada, and S. G. Louie, Electron-phonon coupling from ab initio linear-response theory within the gw method: Correlation-enhanced interactions and superconductivity in ba 1-x k x bio 3, *Physical review letters* **122**, 186402 (2019).
- [32] Z. P. Yin, A. Kutepov, and G. Kotliar, Correlation-enhanced electron-phonon coupling: Applications of gw and screened hybrid functional to bismuthates, chloronitrides, and other high-t c superconductors, *Physical Review X* **3**, 021011 (2013).
- [33] S. Manzeli, D. Ovchinnikov, D. Pasquier, O. V. Yazyev, and A. Kis, 2d transition metal dichalcogenides, *Nature Reviews Materials* **2**, 17033 (2017).
- [34] H. Tan, Y. Liu, Z. Wang, and B. Yan, Charge density waves and electronic properties of superconducting kagome metals, *Physical review letters* **127**, 046401 (2021).
- [35] X. Wang, Y. Yuan, Q.-K. Xue, and W. Li, Charge ordering in high-temperature superconductors visualized by scanning tunneling microscopy, *Journal of Physics: Condensed Matter* **32**, 013002 (2020).